



# Comparative profiling and comprehensive quantification of stratum corneum ceramides in humans and mice by LC/MS/MS<sup>S</sup>

Momoko Kawana, Masatoshi Miyamoto, Yusuke Ohno,<sup>1</sup> and Akio Kihara<sup>1</sup>

Laboratory of Biochemistry, Faculty of Pharmaceutical Sciences, Hokkaido University, Sapporo, Japan

ORCID IDs: 0000-0002-7785-7438 (M.M.); 0000-0003-3702-1043 (Y.O.); 0000-0001-5889-0788 (A.K.)

**Abstract** Ceramides are the predominant lipids in the stratum corneum (SC) and are crucial components for normal skin barrier function. Although the composition of various ceramide classes in the human SC has been reported, that in mice is still unknown, despite mice being widely used as animal models of skin barrier function. Here, we performed LC/MS/MS analyses using recently available ceramide class standards to measure 25 classes of free ceramides and 5 classes of protein-bound ceramides from human and mouse SC. Phytosphingosine- and 6-hydroxy sphingosine-type ceramides, which both contain an additional hydroxyl group, were abundant in the human SC (35% and 45% of total ceramides, respectively). In contrast, in mice, phytosphingosine- and 6-hydroxy sphingosine-type ceramides were present at ~1% and undetectable levels, respectively, and sphingosine-type ceramides accounted for ~90%. In humans, ceramides containing  $\alpha$ -hydroxy FA were abundant, whereas ceramides containing  $\beta$ -hydroxy or  $\omega$ -hydroxy FA were abundant in mice. The hydroxylated  $\beta$ -carbon in  $\beta$ -hydroxy ceramides was in the (*R*) configuration. Genetic knockout of  $\beta$ -hydroxy acyl-CoA dehydratases in HAP1 cells increased  $\beta$ -hydroxy ceramide levels, suggesting that  $\beta$ -hydroxy acyl-CoA, an FA-elongation cycle intermediate in the ER, is a substrate for  $\beta$ -hydroxy ceramide synthesis. **■** We anticipate that our methods and findings will help to elucidate the role of each ceramide class in skin barrier formation and in the pathogenesis of skin disorders.—Kawana, M., M. Miyamoto, Y. Ohno, and A. Kihara. **Comparative profiling and comprehensive quantification of stratum corneum ceramides in humans and mice by LC/MS/MS.** *J. Lipid Res.* 2020. 61: 884–895.

**Supplementary key words** epidermis • fatty acid • lipidomics • mass spectrometry • skin barrier • sphingolipids

This work was supported by Advanced Research and Development Programs for Medical Innovation Grant JP20gm0910002h0006 (A.K.) from the Japan Agency for Medical Research and Development and by KAKENHI Grants JP18H03976 (A.K.) and JP15H05589 (Y.O.) from the Japan Society for the Promotion of Science. The authors declare that they have no conflicts of interest with the contents of this article.

Manuscript received 7 February 2020 and in revised form 1 April 2020.

Published, JLR Papers in Press, April 7, 2020

DOI <https://doi.org/10.1194/jlr.RA120000671>

As an organ covering the body surface, the skin provides a permeability barrier (skin barrier) between organisms and the external environment. The skin barrier prevents excessive water loss, as well as the entry of microorganisms, allergens, and chemical substances. Dysfunction of the skin barrier causes infectious diseases and skin disorders such as atopic dermatitis and ichthyosis (1–3). Skin consists of the epidermis, dermis, and subcutaneous tissue. The epidermis is subdivided into four layers; from the outside inward they are the stratum corneum (SC), stratum granulosum, stratum spinosum, and stratum basale. In the SC, a multilayered lipid structure (lipid lamellae) surrounds corneocytes, terminally differentiated keratinocytes, and plays a central role in skin barrier function. The main constituents of lipid lamellae are ceramides, cholesterol, and FFAs, of which ceramides account for ~50% by weight (4). A variety of classes and molecular species of ceramides exist in lipid lamellae (5–7). The appropriate maintenance of the amount and composition of SC ceramides is important for normal skin barrier function.

Ceramide is composed of a long-chain base (LCB) linked to a FA via an amide bond. Both LCBs and FAs vary in carbon chain length, degree of unsaturation, and the position and number of hydroxyl groups (8). Mammals have five types of LCBs: dihydrosphingosine (DS), sphingosine, phytosphingosine, 6-hydroxy sphingosine, and 4*E*,14*Z*-sphingadiene (4,14-sphingadiene; SD) (Fig. 1A) (8–10). It is currently unclear whether SD is present in the epidermis. The FAs in ceramides can also be classified into five types: nonhydroxy,  $\alpha$ -hydroxy,  $\beta$ -hydroxy,  $\omega$ -hydroxy, and

Abbreviations: DKO, double KO; DS, dihydrosphingosine; EO, esterified  $\omega$ -hydroxy; FPKM, fragments per kilobase of transcript per million mapped reads; HEK, human embryonic kidney; LCB, long-chain base; MRM, multiple reaction monitoring; P-O, protein-bound  $\omega$ -hydroxy; SC, stratum corneum; SD, 4,14-sphingadiene.

<sup>1</sup>To whom correspondence should be addressed.

e-mail: yusuke-ohno@pharm.hokudai.ac.jp (Y.O.);

kihara@pharm.hokudai.ac.jp (A.K.)

**S** The online version of this article (available at <https://www.jlr.org>) contains a supplement.

Copyright © 2020 Kawana et al. Published under exclusive license by The American Society for Biochemistry and Molecular Biology, Inc.

This article is available online at <https://www.jlr.org>

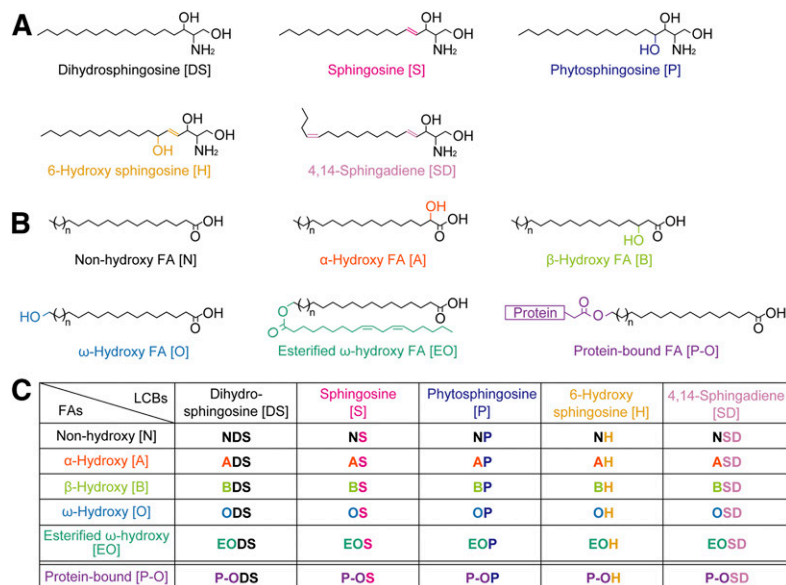


**Fig. 1.** Structures and nomenclature for ceramide classes in mammals. A: Structures of mammalian LCBs. B: FAs constituting mammalian ceramides. C: Nomenclature for 25 free ceramide classes and five P-O ceramide classes. Each ceramide class is represented by a combination of the abbreviations corresponding to its FA and LCB structure.

esterified ω-hydroxy (EO) FAs (Fig. 1B) (8). Although ceramides containing β-hydroxy FA have recently been identified in the mouse epidermis (11, 12), their presence in human skin has not yet been determined. EO ceramides are referred to as ω-O-acylceramides, and a linoleic acid is the predominant FA incorporated into the ω-position of EO ceramides (13, 14). Ceramides are classified into 25 classes according to the different combinations of LCBs and FAs they contain (Fig. 1C). Each ceramide class is designated by a combination of abbreviations that represent the structure of the LCB and FA. For example, the most abundant ceramide class in mammals is composed of sphingosine and nonhydroxy FA and is designated as NS. NS and NDS exist in almost all tissues in mammals, while other ceramide classes exist only in specific tissues. In the human SC, 16 ceramide classes other than SD and β-hydroxy ceramides have been identified (5–7). The alteration of ceramide class composition and reductions in the total amount of ceramides have been observed in the SC of patients with atopic dermatitis (15–17). EO ceramides are epidermis-specific ceramide classes, and their characteristic EO structure is important for the formation and stabilization of lipid organization in the lipid lamellae (18, 19). A portion of EO ceramides are converted into protein-bound ω-hydroxy (P-O) ceramides (Fig. 1B), which are connected to cross-linked proteins constituting the cornified envelope, a structure located beneath the surface of corneocytes (20–22). The impairment of either EO or P-O ceramide production causes ichthyosis (1, 2, 8, 21–26).

Each ceramide class includes a variety of molecular species that differ in FA chain length and/or the degree of unsaturation (8, 27, 28). Therefore, more than several hundred ceramide species exist in the human SC (5–7). The composition of ceramide classes/species in the human SC has previously been analyzed using LC/MS (5–7, 16, 17, 29, 30). However, it is difficult to separately detect and precisely quantify such a tremendous number of ceramide species by LC/MS. Recently, using LC/MS/MS in the multiple reaction monitoring (MRM) mode, which

selects both the molecule-related ion of each lipid species and its specific fragment ion generated by collision-induced dissociation, became a standard technique for specifically detecting and quantifying lipid molecules of interest. However, the following problems must be addressed to develop an LC/MS/MS method for quantifying a variety of ceramide species. First, appropriate internal standards are required. So far, NS with C17:0 FA has generally been used as an internal standard for the quantification of SC ceramides. However, this ceramide is not ideal because it exists endogenously. Additionally, the fragment ion pattern of ceramides differs depending on their LCB moiety (5). Therefore, a ceramide standard for each LCB class is required. However, these standards were not commercially available until recently. Second, ionization of the molecule of interest is often suppressed by coexisting molecules (ion suppression or matrix effects), causing decreased detection sensitivity and inaccurate quantification. Although an SC sample is often collected by tape stripping, the matrix effect caused by coextracted compounds from the tape is unknown. Third, during ionization, the dehydration of ceramide is often induced by in-source decay (31). If the MRM setting has been determined without considering whether the ceramide species of interest is dehydrated, erroneous peak annotation and inaccurate quantification may result. However, the degree of dehydration of each ceramide class has not yet been determined.

Several KO mouse models, lacking genes responsible for the production of ceramides involved in skin barrier formation, have been produced and analyzed (8, 32, 33). In particular, KO mice lacking the genes responsible for EO ceramide production [e.g., the FA elongases *Elovl1* and *Elovl4* (34, 35); the FA ω-hydroxylase *Cyp4f39* (the mouse orthologue of human *CYP4F22*) (26); the ceramide synthase *Cers3* (36); and the transacylase *Pnpla1* (24)] have been used as ichthyosis mouse models to elucidate the pathogenesis of ichthyosis. In addition, the atopic dermatitis mouse model has been used for investigating the correlation between skin barrier function and ceramide

composition (37, 38). Thus, although mice have been generally utilized as a model animal for studying skin barrier function, the ceramide classes measured have primarily been sphingosine-type ceramides such as NS and EOS, and the amounts of other ceramide classes have not yet been elucidated.

Deuterium-labeled standards for each ceramide class have recently become commercially available. In this study, by solving the various problems in the quantification of ceramides through the utilization of these standards, we establish a method that specifically quantifies each ceramide species using LC/MS/MS. Moreover, using this method, we elucidate detailed SC ceramide profiles and determine the differences in ceramide composition between human and mouse SC.

## MATERIALS AND METHODS

### Ethics

This study was approved by the ethics committee of Hokkaido University and performed in accordance with institutional guidelines as well as the Declaration of Helsinki. Written informed consent was obtained from all participants.

### Mice

C57BL/6J mice were purchased from Sankyo Labo Service Corporation (Tokyo, Japan). Mice were housed in a temperature-controlled ( $23 \pm 1^\circ\text{C}$ ) specific pathogen-free environment with a 12 h light/dark cycle and free access to a standard chow diet (PicoLab Rodent Diet 20; LabDiet, St. Louis, MO) and water. The animal experiments were approved by the institutional animal care and use committee of Hokkaido University.

### Chemicals

Deuterium-labeled ceramide standards [*N*-palmitoyl( $d_9$ ) *D*-erythro-sphingosine ( $d_9$ -C16:0 NS), *N*-palmitoyl( $d_9$ ) dihydrosphingosine ( $d_9$ -C16:0 NDS), *N*-palmitoyl( $d_9$ ) *D*-ribo-phytosphingosine ( $d_9$ -C16:0 NP), *N*-palmitoyl( $d_9$ ) 6-(*R*)-hydroxysphingosine ( $d_9$ -C16:0 NH), *N*-(2'-(*R*)-hydroxypalmitoyl( $d_9$ )) *D*-erythro-sphingosine ( $d_9$ -C16:0 AS), *N*-(2'-(*R*)-hydroxypalmitoyl( $d_9$ )) *D*-erythro-sphinganine ( $d_9$ -C16:0 ADS), *N*-(2'-(*R*)-hydroxypalmitoyl( $d_9$ )) *D*-ribo-phytosphingosine ( $d_9$ -C16:0 AP), *N*-(2'-(*R*)-hydroxypalmitoyl( $d_9$ )) 6-(*R*)-hydroxysphingosine ( $d_9$ -C16:0 AH), and *N*-(26-oleoyloxy( $d_9$ ) hexacosanoyl) *D*-erythro-sphingosine (C26:0/ $d_9$ -C18:1 EOS)] and SD were all purchased from Avanti Polar Lipids (Alabaster, AL). *N*- $\omega$ -hydroxytriacontanoyl *D*-erythro-sphingosine (C30:0 OS) was obtained from Cayman Chemical (Ann Arbor, MI). Methanol, acetonitrile, and isopropanol of LC/MS grade, as well as chloroform and ammonium formate of HPLC grade, were all obtained from FUJIFILM Wako Pure Chemical Corporation (Osaka, Japan).

### Collection of SC samples by tape stripping

Human SC samples were collected from healthy volunteers (10 males and 9 females aged 20–50 y). To collect the samples, the inner forearm was first cleaned with water and dried before tape stripping was performed. A  $25 \times 50$  mm piece of film masking tape 465#40 (Teraoka Seisakusho, Tokyo, Japan) was stuck to the inner forearm and then pressed and removed. The procedure was repeated using a new piece of tape. The collected tape samples were applied to an OHP film and stored at  $-30^\circ\text{C}$ . Mouse SC

samples were collected by tape stripping from the back of C57BL/6J mice on the first day after birth using the same procedure as human SC sampling. The second tape strip was used for lipid extraction because the first tape strip may have included dust, detergents, or lotions.

### Lipid analyses by LC/MS/MS

Ceramides were detected and quantified using UPLC coupled with an ESI tandem quadrupole mass spectrometer (Xevo TQ-S; Waters, Milford, MA). LC separation was conducted using a reverse-phase column [ACQUITY UPLC CSH C18 column (particle size, 1.7  $\mu\text{m}$ ; inner diameter, 2.1 mm; length, 100 mm; Waters)] with a binary gradient solvent system as previously described (39). In the positive ion mode, ionization was performed using the following parameters: capillary voltage, 2.5 kV; cone voltage, 30 V for nonhydroxy,  $\alpha$ -hydroxy,  $\beta$ -hydroxy, and  $\omega$ -hydroxy ceramides or 46 V for EO ceramides; source temperature,  $140^\circ\text{C}$ ; desolvation temperature,  $650^\circ\text{C}$ ; desolvation gas flow, 1,200 l/h; and nebulizer gas, 7.0 bar. In the negative ion mode, capillary voltage and cone voltage were set at 2.0 kV and 30 V, respectively, and the other parameters were the same as in the positive ion mode. Each ceramide species was detected in the MRM mode using optimized *m/z* values of precursor ions (Q1) and product ions (Q3) and collision energies (supplemental Table S1).  $[\text{M}-\text{H}_2\text{O} + \text{H}]^+$  was selected as a precursor ion to detect NS, NH, NSD, AS, BS, AH, and ASD ceramides, and  $[\text{M} + \text{H}]^+$  was selected to detect NDS, NP, ADS, and AP ceramides. Both  $[\text{M} + \text{H}]^+$  and  $[\text{M}-\text{H}_2\text{O} + \text{H}]^+$  were selected to detect  $\omega$ -hydroxy and EO ceramides. Ceramides were quantified by calculating the ratio of the peak area of each ceramide species compared with that of the deuterium-labeled ceramide (internal standard) corresponding to each ceramide class. SD ceramides were quantified using a deuterium-labeled sphingosine-type ceramide standard because deuterium-labeled SD ceramides are commercially unavailable. EO and  $\omega$ -hydroxy ceramides were quantified using the deuterium-labeled  $\alpha$ -hydroxy ceramide standards that shared common LCB structures. MassLynx software (Waters) was used for data analysis.

### Evaluation of matrix effect

Fresh tape, not including the SC, was cut and transferred into a glass tube containing 2 ml methanol. After sonication (room temperature, 5 min), the tape was removed. The tube was centrifuged (2,600 g, room temperature, 5 min), and the supernatant was recovered to a new glass tube and evaporated. Tape extracts were dissolved in 100  $\mu\text{l}$  chloroform-methanol (1:2; v/v) containing deuterium-labeled ceramide standards (10 pmol each), and each ceramide standard was detected by LC/MS/MS.

### Lipid extraction

Tape strips that included the SC were cut to a size of  $5 \times 10$  mm and transferred into a glass tube containing 400  $\mu\text{l}$  methanol. As internal standards, deuterium-labeled ceramide standards were added to human SC samples as follows:  $d_9$ -C16:0 NS, 0.5 pmol;  $d_9$ -C16:0 NDS, 1 pmol;  $d_9$ -C16:0 NP, 5 pmol;  $d_9$ -C16:0 NH, 5 pmol;  $d_9$ -C16:0 AS, 0.5 pmol;  $d_9$ -C16:0 ADS, 0.5 pmol;  $d_9$ -C16:0 AP, 2 pmol; and  $d_9$ -C16:0 AH, 2 pmol. To mouse SC samples the following standards were added:  $d_9$ -C16:0 NS, 5 pmol;  $d_9$ -C16:0 NDS, 10 pmol;  $d_9$ -C16:0 NP, 1 pmol;  $d_9$ -C16:0 NH, 0.5 pmol;  $d_9$ -C16:0 AS, 2 pmol;  $d_9$ -C16:0 ADS, 0.5 pmol;  $d_9$ -C16:0 AP, 0.5 pmol; and  $d_9$ -C16:0 AH, 0.5 pmol. After sonication (room temperature, 5 min), the tape was removed. To remove the SC pellet, the tube was centrifuged (2,600 g, room temperature, 5 min). The supernatant was recovered to a new glass tube and dried (total free lipid samples). The SC pellet was subjected to extraction of P-O ceramides as follows. To remove free lipids completely, 400  $\mu\text{l}$  methanol was added, vigorously mixed, and centrifuged (2,600 g,

room temperature, 5 min). After the supernatant was removed, the same procedure was repeated twice, and the samples were then incubated with 400  $\mu$ l 95% methanol (60°C, 2 h). After centrifugation (20,400 g, room temperature, 3 min), the supernatant was removed. The pellet was again incubated with 400  $\mu$ l 95% methanol (60°C, 2 h), followed by centrifugation (2,600 g, room temperature, 5 min) and removal of the supernatant. To release P-O ceramides, 400  $\mu$ l 1 M potassium hydroxide in 95% methanol and internal standards were added to human samples as follows:  $d_9$ -C16:0 AS, 1 pmol;  $d_9$ -C16:0 ADS, 0.25 pmol;  $d_9$ -C16:0 AH, 1 pmol; and  $d_9$ -C16:0 AP, 0.25 pmol. To mouse samples the following standards were added:  $d_9$ -C16:0 AS, 5 pmol;  $d_9$ -C16:0 ADS, 0.5 pmol;  $d_9$ -C16:0 AH, 0.25 pmol; and  $d_9$ -C16:0 AP, 0.25 pmol. The solutions were incubated at 60°C for 2 h. For neutralization, 400  $\mu$ l 1 M acetic acid was added. After the addition of 400  $\mu$ l chloroform, the samples were vigorously mixed for 1 min and centrifuged (2,600 g, room temperature, 5 min). The resulting organic phase (lower phases) was recovered and dried (P-O ceramide samples). Total free lipid samples and P-O ceramide samples were dissolved in 100 and 50  $\mu$ l chloroform-methanol (1:2; v/v), respectively, and subjected to LC/MS/MS analyses.

Lipid extractions from the mouse epidermis were performed as previously described (28). Lipids were extracted from cultured cells as follows. Cells cultured in a six-well plate were washed twice with 1 ml PBS, detached from the plate using a scraper, and transferred into plastic tubes. After centrifugation (400 g, 4°C, 3 min), the supernatants were removed. The cells were suspended in 100  $\mu$ l PBS and mixed with 375  $\mu$ l chloroform-methanol-12 M formic acid (100:200:1; v/v/v) and an internal standard ( $d_9$ -C16:0 AS, 10 pmol). Samples were mixed with 125  $\mu$ l chloroform and 125  $\mu$ l water and centrifuged (20,400 g, room temperature, 3 min). The organic phase was recovered and dried. Lipids were dissolved in 500  $\mu$ l chloroform-methanol (1:2; v/v) and subjected to LC/MS/MS analyses.

### Cell culture and transfection

HAP1 cells are near-haploid human cells derived from a chronic myelogenous leukemia sample (40). *HACD1* and *HACD2* double KO (DKO) HAP1 cells and their control cells have previously been described (41). These HAP1 derivatives were cultured in Iscove's Modified Dulbecco's Medium (Thermo Fisher Scientific, Waltham, MA). Human embryonic kidney (HEK) 293T cells were grown in DMEM (D6429; Merck, Darmstadt, Germany) in dishes coated with 0.1 mg/ml collagen (Cellmatrix type I-P; Nitta Gelatin, Osaka, Japan). Each medium was supplemented with 10% FBS (Thermo Fisher Scientific), 100 units/ml penicillin, and 100  $\mu$ g/ml streptomycin (Merck). Cells were cultured at 37°C under 5% CO<sub>2</sub>. Transfections were performed using ViaFect Transfection Reagent (Promega, Madison, WI) according to the manufacturer's instructions.

### In vitro ceramide synthesis

HEK 293T cells were transfected with either pCE-puro 3 $\times$ FLAG-CERS1 or pCE-puro 3 $\times$ FLAG-CERS5, which are the plasmids designed for the expression of N-terminally 3 $\times$ FLAG-tagged human ceramide synthase CERS1 or CERS5, respectively, in mammalian cells. Twenty-four hours after transfection, the cells were washed twice with PBS, suspended in lysis buffer [50 mM HEPES/NaOH (pH 7.4), 150 mM NaCl, 1 mM MgCl<sub>2</sub>, 1 mM DTT, 1 mM PMSF, 1 $\times$  protease inhibitor cocktail (cOmplete, EDTA-free; Merck)], and lysed by sonication. Cell debris was removed by centrifugation (400 g, 4°C, 3 min), and the resulting supernatant was subjected to ultracentrifugation (100,000 g, 4°C, 35 min). The pellet (membrane fraction) was suspended in lysis buffer. For NSD synthesis, the membrane fraction (50  $\mu$ g) prepared from the cells overexpressing CERS5 was mixed with 1  $\mu$ M SD and

1  $\mu$ M C16:0-CoA (Merck) (total volume: 50  $\mu$ l) and incubated (37°C, 30 min). For BS synthesis, a 20  $\mu$ g membrane fraction, prepared from the cells overexpressing CERS1 (for C18:0 BS synthesis) or CERS5 (for C14:0 BS synthesis), was mixed with 5  $\mu$ M  $d_7$ -sphingosine (Avanti Polar Lipids), 5  $\mu$ M  $\beta$ -hydroxy FAs [ $\beta$ -hydroxy C18:0 (3-hydroxyoctadecanoic acid; Cayman Chemical),  $\beta$ -hydroxy C14:0 (3-hydroxymyristic acid; Tokyo Chemical Industry, Tokyo, Japan), or (*R*)- $\beta$ -hydroxy C14:0 (3*R*-hydroxymyristic acid; Toronto Research Chemicals, North York, Canada)], 400  $\mu$ M CoA, 20 mM ATP, 150 mM NaCl, and 1 mM MgCl<sub>2</sub> (total volume: 50  $\mu$ l) and incubated at 37°C for 30 min. The reactions were terminated by the addition of 187.5  $\mu$ l chloroform-methanol-12 M formic acid (100:200:1; v/v/v) and vigorous mixing for 1 min. After the addition of 62.5  $\mu$ l chloroform and 62.5  $\mu$ l H<sub>2</sub>O, phases were separated by centrifugation (20,000 g, room temperature, 3 min). The organic phase was recovered and dried. Lipids were dissolved in 100  $\mu$ l chloroform-methanol (1:2; v/v), and the synthesized ceramides were detected by LC/MS/MS.

## RESULTS

### Establishment of the method that specifically detects ceramide species by LC/MS/MS

To develop a method for distinguishing each ceramide species by LC/MS/MS, we first performed product ion scanning using deuterium-labeled ceramide standards ( $d_9$ -ceramide; containing nine deuteriums instead of protiums in its FA moiety). By fragmentation of NS and NH, product ions of  $m/z$  264 and 280, which correspond to sphingosine and 6-hydroxy sphingosine moieties, respectively, were predominantly generated (Fig. 2A). The dissociation of NP yielded three major product ions ( $m/z$  264, 282, and 300) at similar intensities, of which two product ions ( $m/z$  264 and 282) overlapped with the major and minor product ions of NS, respectively, indicating that the product ion of  $m/z$  300 was specific to phytosphingosine-type ceramide. Product ions of  $m/z$  266 and 284 were mainly produced by the fragmentation of NDS, and neither were detected in other ceramide classes. Because the NSD standard was not commercially available, we synthesized C16:0 NSD by incubating C16:0-CoA and SD with membrane fraction prepared from HEK 293T cells. NSD was predominantly cleaved to a fragment ion of  $m/z$  262, which corresponded to the SD moiety (Fig. 2B). Next, to investigate whether the difference in an FA moiety affected the fragmentation of ceramide, we performed fragmentation analyses using AS and EOS standards. The MS/MS spectrum of both standards were the same as that of NS (Fig. 2C), indicating that the difference in the FA moiety did not affect the generation of the fragment ion derived from the LCB moiety. Recently, BS, which is composed of a  $\beta$ -hydroxy FA and sphingosine, has been identified in mouse epidermis (11, 12). Because AS and BS are structural isomers, in the positive ion mode, BS is predicted to be detected at a different retention time using the same MRM settings as AS detection. In LC/MS/MS analysis using the MRM setting to detect C26:0 AS, C26:0 AS was detected in the human SC (13.20 min), while a large peak at an earlier retention time (12.86 min), instead of C26:0 AS, was detected in the

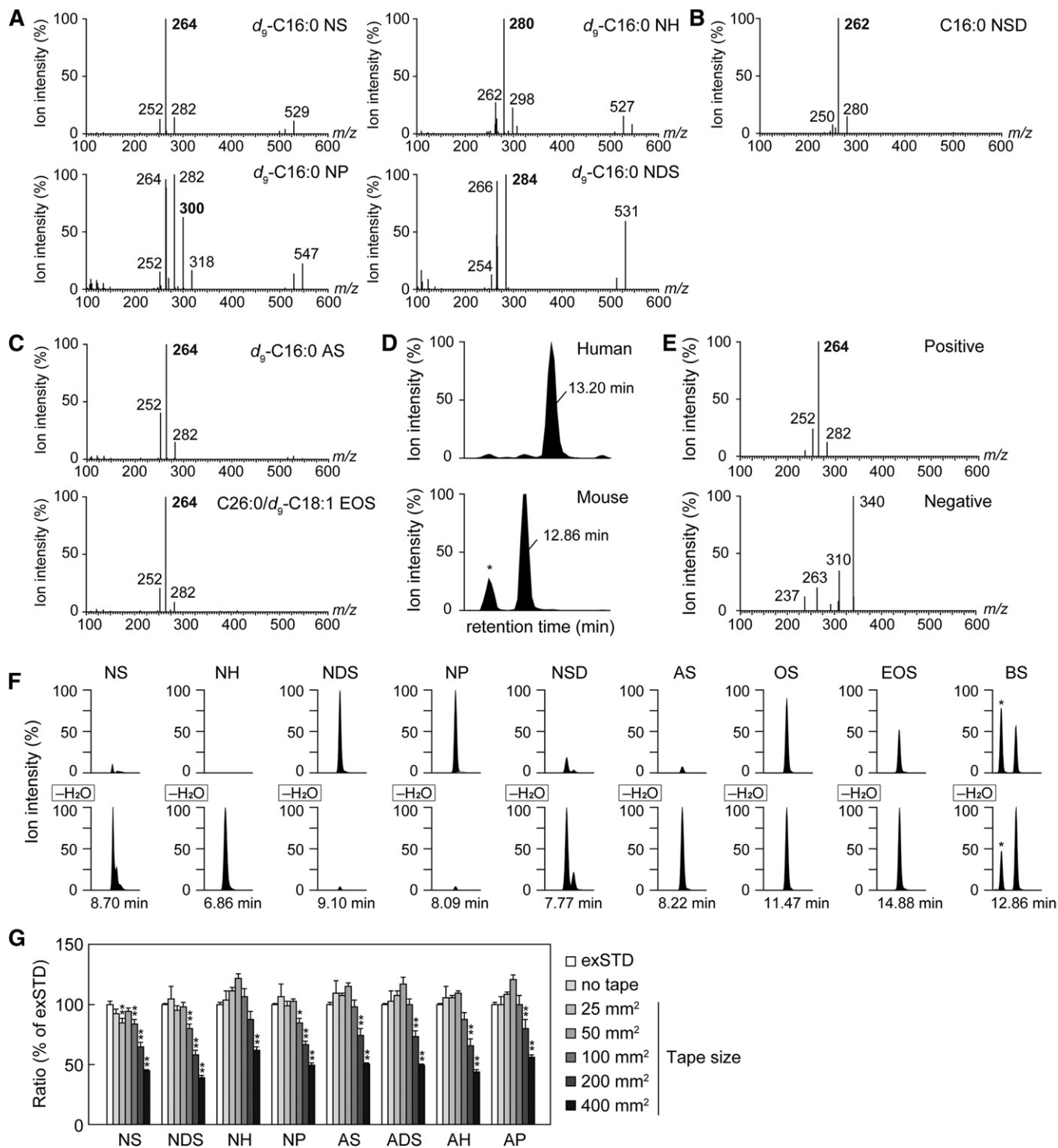


**Fig. 2.** Optimization of SC ceramide analysis using LC/MS/MS. A–C: Product ion scanning was performed using ceramide standards in the positive ion mode (A:  $d_9$ -C16:0 NS,  $d_9$ -C16:0 NDS,  $d_9$ -C16:0 NH, and  $d_9$ -C16:0 NP; B: C16:0 NSD; and C:  $d_9$ -C16:0 AS and C26:0/ $d_9$ -C18:1 EOS). The  $m/z$  values of each precursor ion were set as follows:  $d_9$ -C16:0 NS, 547.5;  $d_9$ -C16:0 NDS, 549.5;  $d_9$ -C16:0 NH, 563.5;  $d_9$ -C16:0 NP, 565.5; C16:0 NSD, 536.5;  $d_9$ -C16:0 AS, 563.5; and C26:0/ $d_9$ -C18:1 EOS, 967.9. Fragment ions were detected in the scanning range  $m/z$  100–600. The values shown in bold represent the  $m/z$  of a fragment ion specific for each ceramide class. C16:0 NSD was synthesized by incubating 1  $\mu$ M SD and 1  $\mu$ M C16:0-CoA with membrane fractions (50  $\mu$ g) prepared from HEK 293T cells overexpressing CERS5 at 37°C for 1 h (B). D: Lipids were extracted from the human SC and mouse epidermis and subjected to LC/MS/MS analysis using the MRM setting to detect C26:0 AS. \*Unidentified peak. E: Product ion scanning of C26:0 BS was performed in the positive ion mode (upper) and negative ion mode (lower). F: MRM analyses were performed by setting the  $m/z$  values of  $[M + H]^+$  (upper panel) and  $[M - H_2O + H]^+$  (lower panel) at Q1 and the  $m/z$  values of a fragment ion specific for each LCB at Q3. The values below the horizontal axis represent the retention time of each peak. \*Unidentified peak. G: Each  $d_9$  ceramide standard was added to the extract from the indicated size of tape piece (the final volumes of all samples were adjusted to 100  $\mu$ l) and detected by LC/MS/MS. Values are the detection rate compared with the external standards (exSTD) and represent means  $\pm$  SDs ( $n = 3$ ; \* $P < 0.05$  and \*\* $P < 0.01$ ; Dunnett's test).

mouse epidermis (Fig. 2D). The MS/MS spectrum of this peak (12.86 min) in the positive ion mode was similar to that of NS (Fig. 2E), indicating that the peak was derived from sphingosine-type ceramide. In the negative ion mode, four product ions ( $m/z$  340, 310, 263, and 237) were generated with the highest intensity at  $m/z$  340. The fragmentation pattern of this peak is consistent with that of C26:0 BS in previous reports (12, 42), demonstrating that the peak detected at 12.86 min was C26:0 BS. In summary, the ceramide classes containing sphingosine, 6-hydroxy sphingosine, phytosphingosine, DS, and SD are distinguished in MRM analyses by selecting product ions of  $m/z$  264, 280, 300, 284, and 262, respectively. In addition, ceramide species having different FA moieties are separated by the differences in  $m/z$  of their precursor ions and their retention time in the LC.

Ceramides are dehydrated by in-source decay during ionization (31). Due to dehydration, the  $m/z$  value of some ceramide species may become the same  $m/z$  as another ceramide species. For example, the  $m/z$  value of  $[C24:0 AS-H_2O + H]^+$  is 648, which has the same  $m/z$  as that of  $[C24:1 NS + H]^+$ ; that is, the peaks derived from different ceramide species are detected in the same MRM settings. Therefore, differences in the susceptibility to dehydration may cause erroneous peak annotation and inaccurate quantification. To examine the differences in the degree of dehydration among ceramide classes, we performed LC/MS/MS analyses with MRM settings in which both  $[M + H]^+$  and  $[M-H_2O + H]^+$  were selected as precursor ions. Ceramide classes with double bond(s) in their LCB (NS, NH, and NDS) were highly dehydrated, while those without double bonds (NDS and NP) were not (Fig. 2F). Dehydrated AS was also detected predominantly, whereas nondehydrated OS was detected at the same levels as dehydrated OS. The nondehydrated EOS and BS levels were about half of the dehydrated levels. From these results, we quantified ceramides using MRM settings in which a dehydrated type, a nondehydrated type, or both types were selected, depending on the specific ceramide class.

Tape stripping is often conducted to collect SC samples. However, certain ingredients in the tape are coextracted with lipids and may cause a matrix effect. To investigate the effect of the extracts derived from the tape on the detection of ceramides,  $d_9$  ceramide standards were mixed with the tape extracts and detected by LC/MS/MS. Compared with the standards diluted only with methanol (external standards), the detection ratio of each  $d_9$  ceramide mixed with tape extracts was decreased, especially in the extracts from 200 and 400 mm<sup>2</sup> pieces of tape (Fig. 2G). The extracts from 25 and 50 mm<sup>2</sup> pieces of tape did not affect the detection ratio. From this result, although a matrix effect (suppression of ionization) is caused by the tape-derived coextracts, this effect can be nullified by reducing the tape size to 50 mm<sup>2</sup> or less.

#### Different SC ceramide classes and FA composition between humans and mice

Using the extraction protocol and the LC/MS/MS settings determined in Fig. 2, we measured ceramides in human and mouse SC. The SC specimens were collected via

tape stripping from mice on the first day after birth (to avoid hair) and humans. Lipids were extracted,  $d_9$  ceramides were added as internal standards, and each ceramide species was quantified by LC/MS/MS. We successfully quantified 21 classes of ceramides from the human SC (NS, NDS, NH, NP, NSD, AS, ADS, AH, AP, ASD, BS, OS, ODS, OH, OP, OSD, EOS, EODS, EOH, EOP, and EOSD), including 345 species; and 16 classes from the mouse SC (NS, NDS, NP, NSD, AS, ADS, ASD, BS, OS, ODS, OP, OSD, EOS, EODS, EOP, and EOSD), including 268 species (Fig. 3A, B; supplemental Table S2). In the human SC, NP, NH, and AH were abundant (24.2%, 23.7%, and 18.0% of total ceramides, respectively), followed by AP, NDS, NS, AS, EOH, EOS, EOP, and ADS (in descending order, 1% to 9%). The proportions of other ceramide classes were lower than 1%. In the mouse SC, NS levels were the highest (57.9% of total ceramides), followed by EOS, NDS, OS, and BS in that order (4% to 16%). The proportions of other ceramide classes were lower than 2%. Of the categories of ceramide classes that contain a common LCB, 6-hydroxy sphingosine- and phytosphingosine-type ceramides were abundant in the human SC (45.4% and 34.7% of total ceramides, respectively) (Fig. 3C). On the other hand, the proportion of the sphingosine-type ceramide class was highest in the mouse SC (87.7%). The proportion of the phytosphingosine-type ceramide class in mice was low (1.2%), and the 6-hydroxy sphingosine-type ceramide class undetectable, in mice. SD-type ceramide levels were quite low (~0.4%) both in humans and mice. Of the categories of ceramide classes that have the same type of FA, the proportion of the nonhydroxy ceramide class was the highest (59.4%) in the human SC, followed by  $\alpha$ -hydroxy ceramides (32.5%), EO ceramides (6.3%), and  $\omega$ -hydroxy ceramides (1.6%) (Fig. 3D). Trace amounts of  $\beta$ -hydroxy ceramides were present in the human SC (0.17%). Although nonhydroxy ceramide was the principal ceramide class present in both the mouse (68.9%) and human (59.4%) SC, the proportions of the other ceramide classes were largely different between mice and humans. In mice, the EO,  $\omega$ -hydroxy, and  $\beta$ -hydroxy ceramide classes were 16.9%, 8.7%, and 4.9%, respectively, and  $\alpha$ -hydroxy ceramide, the second highest ceramide class in humans, was quite low (0.7%). Thus, the composition of SC ceramide classes was largely different between humans and mice.

Various ceramide species with different FA chain lengths exist in each ceramide class. We next compared FA composition among ceramide classes that exceeded 1% of the total ceramides (10 and 6 classes in humans and mice, respectively) (Fig. 3E). Generally, the FA chain length of  $\omega$ -hydroxylated ceramides (EO and  $\omega$ -hydroxy) was C30–C34, and that of the other ceramides was C16–C30. Major FAs of nonhydroxy ceramides were C26:0 > C24:0 > C28:0 both in human and mouse SC (except for human NDS, which was C24:0 > C26:0 > C28:0). The FA compositions of the human AH, AP, and mouse BS were C26:0 > C24:0 > C25:0; C24:0 > C26:0 > C25:0; and C26:0 > C28:0 > C25:0, respectively. C26:0 and C24:0 were the top two FAs in most ceramide classes, other than  $\omega$ -hydroxy or EO ceramides, although C16:0 was the principal ceramide present in

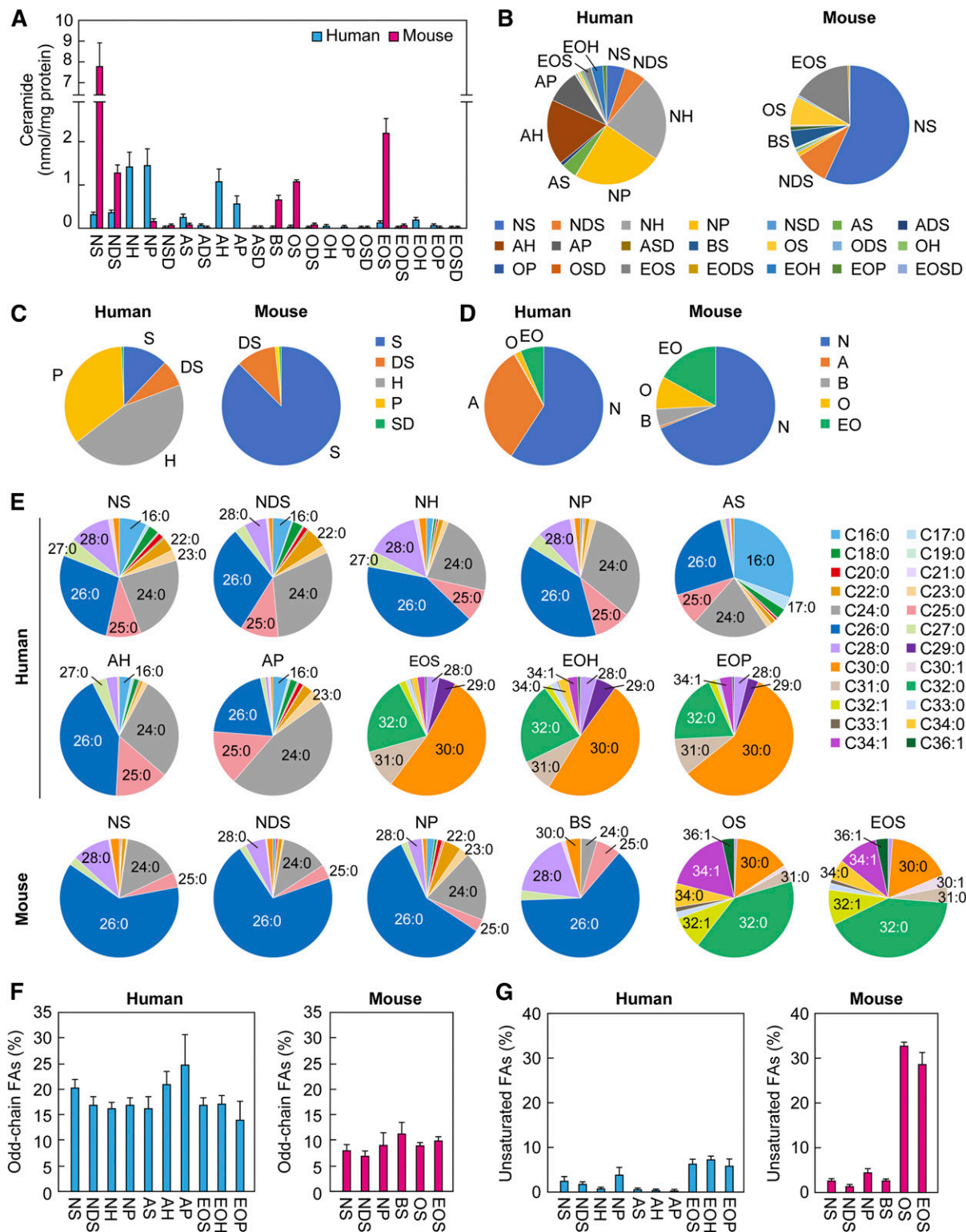


**Fig. 3.** Ceramide profiles in human and mouse SC. SC samples were collected by tape stripping from humans (aged 20–50 years;  $n = 19$ ) and mice (on the first day after birth;  $n = 3$ ). Lipids were extracted from the tapes and subjected to LC/MS/MS analyses to quantify ceramides. A: Amount of each ceramide class. Values are the sum of the ceramide species containing each FA chain length (nonhydroxy ceramides,  $\alpha$ -hydroxy ceramides, and BS; C14–C36;  $\omega$ -hydroxy and EO ceramides: C26–36) and represent means  $\pm$  SDs. B: The ratio of each ceramide class to total ceramides. C: The proportion of ceramide classes containing a common LCB. D: The ratio of ceramide classes containing a common type of FA. E: The FA composition of ceramide classes representing more than 1% of the total ceramides in human and mouse SC. F: The ratio of odd-chain FAs in each ceramide class. Values represent means  $\pm$  SDs. G: The ratio of unsaturated FAs in each ceramide class. Values represent means  $\pm$  SDs.

human AS (C16:0 > C26:0 > C24:0). Human EO ceramides (EOS, EOH, and EOP) were composed of C30:0 > C32:0 > C31:0. Mouse EOS and OS contained C32:0 > C30:0 > C34:1 and C32:0 > C34:1 > C30:0, respectively. Although the levels of ceramides containing odd-chain FAs are generally low in a broad range of tissues, those containing odd-chain FAs such as C25, C27, C29, and C31 were present at relatively high levels both in human and mouse SC. In particular, the levels of C25:0 AH, C25:0 AP, and C31:0 EO ceramides (EOS, EOH, and EOP) in humans were the third highest ceramide species in each ceramide class. The total percentage of ceramides with odd-chain FAs were 14% to 25% in human and 6% to 10% in mouse ceramide classes (Fig. 3F). Unsaturated FAs in the nonhydroxy,  $\alpha$ -hydroxy, and  $\beta$ -hydroxy ceramide classes were low (0.3% to 4% in humans and 1% to 4% in mice), while those in the EO and  $\omega$ -hydroxy ceramide classes were high (5% to 7% in humans and 29% to 33% in mice), especially mouse C34:1 EOS (10.5%) (Fig. 3G). Overall, there were no remarkable differences in the FA chain length of ceramides between human and mouse SC.

### Protein-bound ceramides in human and mouse SC

Unlike plasma membranes in general, which are constituted by a lipid bilayer, corneocytes are covered by a lipid monolayer mainly composed of P-O ceramides (20), which are presumed to link corneocytes to the lipid lamellae. To investigate the amount and composition of P-O ceramides in human and mouse SC, P-O ceramides were quantified by LC/MS/MS analyses. Consistent with earlier reports (43, 44), in humans, P-OS was predominant (64% of total P-O ceramides), followed by P-OH (28%) (Fig. 4A; supplemental Tables S4, S5). In mice, P-OS was also the most abundant (84%) P-O ceramide class. FA species that constituted P-OS were C30–C34 (C30:0 > C32:0 > C32:1 in humans and C34:1  $\approx$  C32:0 > C32:1 in mice) (Fig. 4B). There were no clear differences in FA composition among P-O ceramide classes with different LCBs, both in humans and mice (supplemental Table S5). Although semiquantitative analysis of P-O ceramides by TLC and quantification of limited P-O ceramide species by LC/MS/MS have already been conducted (44–46), we successfully quantified 63 and 74 P-O ceramide species in humans and mice, respectively, leading to the elucidation of the detailed composition of P-O ceramides.

### (R) configuration of the hydroxylated $\beta$ -carbon in BS

The structural configuration of the hydroxylated  $\beta$ -carbon in BS, a ceramide class moderately present in the mouse SC (Fig. 3), is unknown. To determine its configuration, we first synthesized C18:0 BS by incubating (*R, S*)  $\beta$ -hydroxy C18:0 FA and *d*<sub>7</sub> sphingosine with the membrane fraction prepared from HEK 293T cells overexpressing CERS1 (a ceramide synthase that shows high activity against C18:0 acyl-CoA) and performed LC/MS/MS analysis. In the LC chromatogram of the synthesized (*R, S*) C18:0 BS, two peaks were observed at 8.63 and 8.78 min, and the latter peak was identical with C18:0 BS in the mouse epidermis (Fig. 5A). Because neither (*R*) nor (*S*)  $\beta$ -hydroxy C18:0

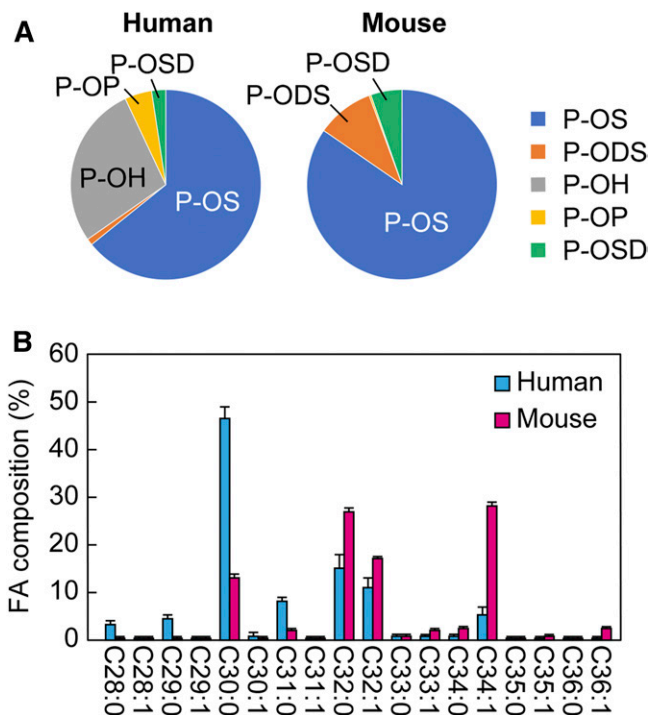


**Fig. 4.** P-O ceramide profiles in human and mouse SC. P-O ceramides were extracted from the SC samples collected by tape stripping from humans (aged 20–50 years;  $n = 19$ ) and mice (on the first day after birth;  $n = 3$ ) and quantified by LC/MS/MS analyses. A: The ratio of each P-O ceramide class to the total P-O ceramides. B: FA composition of P-OS. Values represent means  $\pm$  SDs.

FAs were commercially available, we could not determine the structural configuration of the two peaks. Next, we synthesized (*R, S*) C14:0 BS and (*R*) C14:0 BS by mixing (*R, S*)  $\beta$ -hydroxy C14:0 FA and (*R*)  $\beta$ -hydroxy C14:0 FA, respectively, with *d*<sub>7</sub> sphingosine and the membrane fraction prepared from HEK 293T cells overexpressing CERS5 (a ceramide synthase that exhibits high activity against C14:0 acyl-CoA). In the LC chromatogram of (*R, S*) C14:0 BS, two peaks (6.88 and 7.04 min) were again detected (Fig. 5B). Although two peaks (6.79 and 6.96 min) were also observed in (*R*) C14:0 BS, the latter peak was larger than the former, indicating that the former and latter peaks corresponded to (*S*) BS and (*R*) BS, respectively. The reason why (*S*) C14:0 BS was detected despite the use of (*R*)  $\beta$ -hydroxy C14:0 FA may be due to the isomerization of (*R*) to (*S*) or the contamination of (*S*)  $\beta$ -hydroxy C14:0 FA in (*R*)  $\beta$ -hydroxy C14:0 FA. From these results, we concluded that the structural configuration of the hydroxylated  $\beta$ -carbon in BS is in the (*R*) configuration.

### Involvement of the FA elongation cycle in BS synthesis

The FA elongation cycle in the ER membrane produces FAs with  $\geq$ C18 chain lengths. In this cycle, FA is elongated in the form of acyl-CoAs, and  $\beta$ -hydroxy acyl-CoA is generated as an intermediate (Fig. 6A) (27, 47). Although the synthesis pathway of BS has not yet been identified, we suspected that  $\beta$ -hydroxy acyl-CoAs in the FA elongation cycle are used for BS production because ceramide synthesis also proceeds in the ER membrane. In the FA elongation cycle,



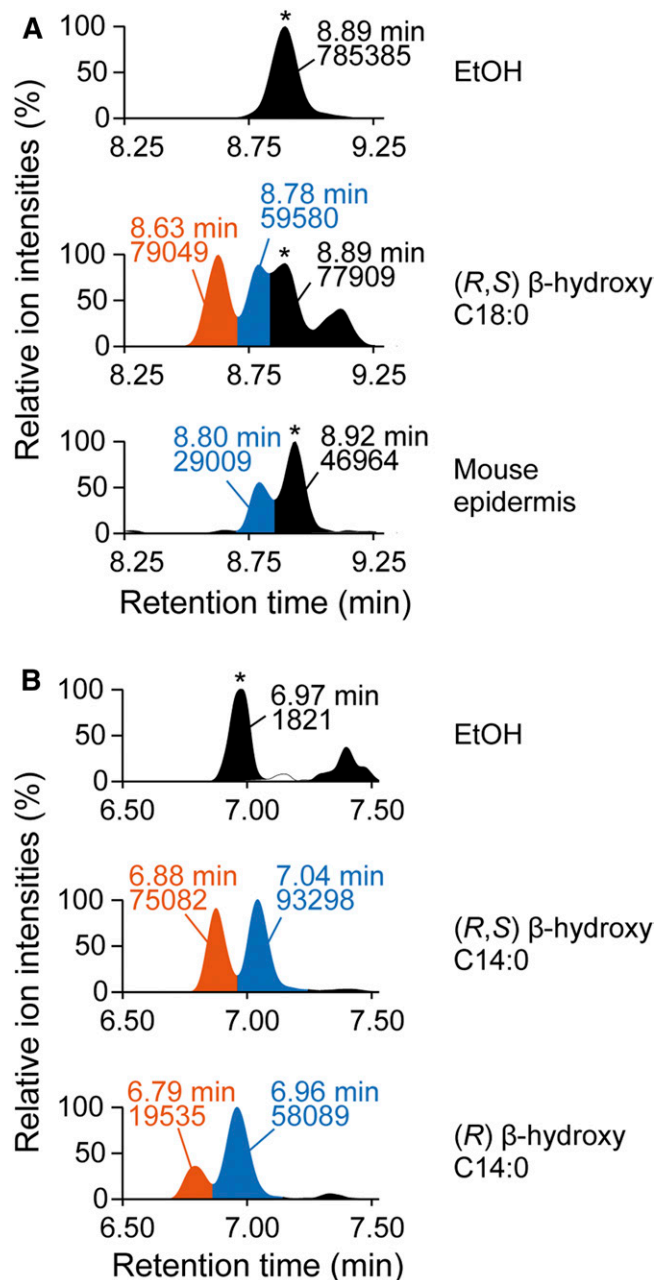


**Fig. 5.** (*R*) configuration of hydroxylated  $\beta$ -carbon in BS. **A:** Membrane fractions (20  $\mu$ g) prepared from HEK 293T cells over-expressing CERS1 were incubated with EtOH or 5  $\mu$ M (*R,S*)  $\beta$ -hydroxy C18:0 FA and 5  $\mu$ M  $d_7$  sphingosine at 37°C for 1 h to produce C18:0 BS. Lipids were extracted and subjected to LC/MS/MS analysis to detect C18:0 BS containing  $d_7$ -labeled sphingosine [upper, EtOH; middle, (*R,S*)  $\beta$ -hydroxy C18:0 FA; and lower, C18:0 BS in mouse epidermis]. \*Unidentified peak. **B:** Membrane fractions (20  $\mu$ g) prepared from HEK 293T cells over-expressing CERS5 were incubated with EtOH, 5  $\mu$ M (*R,S*)  $\beta$ -hydroxy C14:0 FA, or (*R*)  $\beta$ -hydroxy C14:0 FA and 5  $\mu$ M  $d_7$  sphingosine at 37°C for 1 h. Lipids were extracted and subjected to LC/MS/MS analysis to detect C14:0 BS containing  $d_7$ -labeled sphingosine [upper, EtOH; middle, (*R,S*)  $\beta$ -hydroxy C14:0 FA; and lower, (*R*)  $\beta$ -hydroxy C14:0 FA]. \*Unidentified peak. The vertical axis of each chromatogram shows relative intensity. The values represented in the chromatogram indicate retention time (upper) and peak area (lower). EtOH, ethanol.

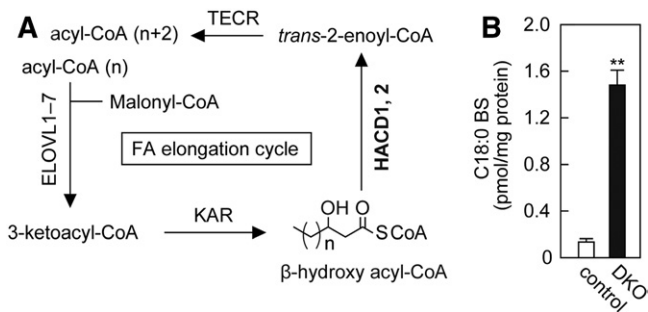


**Fig. 6.** Increase in BS levels due to the accumulation of  $\beta$ -hydroxy acyl-CoAs, which are intermediates in the FA elongation cycle. **A:** The FA elongation cycle localized in the ER produces acyl-CoAs having  $\geq$ C18 chain lengths. In each cycle, the chain length of the substrate acyl-CoA is elongated by two carbon chains through a four-step reaction. The enzymes involved in each reaction step and intermediates are depicted.  $\beta$ -Hydroxy acyl-CoA dehydratases HACD1 and HACD2 convert  $\beta$ -hydroxy acyl-CoAs to *trans*-2-enoyl-CoAs. **B:** Lipids were extracted from control and *HACD1 HACD2* DKO HAP1 cells, and C18:0 BS was quantified by LC/MS/MS. Values represent means  $\pm$  SDs ( $n = 3$ ; \*\* $P < 0.01$ ; two-tailed Student's *t*-test).

$\beta$ -hydroxy (3-hydroxy) acyl-CoA dehydratase HACD1 or HACD2 converts  $\beta$ -hydroxy acyl-CoAs to *trans*-2-enoyl-CoAs (41, 48). To investigate the involvement of the FA elongation cycle in BS synthesis, we measured BS levels in *HACD1 HACD2* DKO HAP1 cells, in which  $\beta$ -hydroxy acyl-CoAs accumulate. The amount of BS was increased in *HACD1 HACD2* DKO cells by 15-fold compared with control cells (Fig. 6B), suggesting that the  $\beta$ -hydroxy FA moiety of BS is derived from the FA elongation cycle.

## DISCUSSION

Elucidation of the detailed compositions of SC ceramides is important in understanding the mechanisms underlying skin barrier formation and the pathogenesis of skin disorders. In the current study, we performed LC/MS/MS analyses and quantified free ceramides (21 classes/345 species in humans; 16 classes/268 species in mice) and P-O ceramides (5 classes/63 species in humans; 5 classes/74 species in mice) (Figs. 3, 4; supplemental Tables S2–S5), revealing the in-depth ceramide profiles of human and mouse SC.

The ratio of each ceramide class to total ceramides in this study was not largely different from earlier studies (supplemental Table S6). Although the amounts of SD-type ceramides and BS were previously unknown, we determined them for the first time (Fig. 3; supplemental Tables S2, S3). A variety of ceramide species, including phytosphingosine- and 6-hydroxy sphingosine-type ceramides, existed abundantly in the human SC. On the other hand, phytosphingosine- and 6-hydroxy sphingosine-type ceramides were at very low and undetectable levels, respectively, in the mouse SC (Fig. 3; supplemental Tables S2, S3). The types of hydroxylated FAs in the human SC ceramides were also different from those in the mouse SC ceramides; in humans,  $\alpha$ -hydroxy ceramides were abundant, and BS and

$\omega$ -hydroxy ceramides were almost absent; while in mice, only small amounts of  $\alpha$ -hydroxy ceramides were present, and instead BS and  $\omega$ -hydroxy ceramides existed at relatively high levels (Fig. 3; supplemental Tables S2, S3). Therefore, it is likely that in mice other types of hydroxylated ceramides (BS and  $\omega$ -hydroxy ceramides) compensate for the functions of human hydroxylated ceramides (phyto-sphingosine-, 6-hydroxy sphingosine-, and  $\alpha$ -hydroxy-type ceramides). The hydroxyl groups may enhance the interactions between lipids by forming hydrogen bonds, even if they are present at different positions, and may also contribute to the formation and maintenance of lipid lamellae, which have a pivotal role in skin barrier formation.


Sphingosine- and phytosphingosine-type ceramides are generated either via desaturation between the 4 and 5 positions of the LCB moiety of dihydroceramides (DS ceramides) by the desaturase *DEGS1*, or via hydroxylation of the same moiety at the 4 position by the hydroxylase *DEGS2* (49, 50). The difference in phytosphingosine-type ceramide levels between humans and mice may be due to the difference of expression levels of *DEGS2*. In transcriptome analysis of human skin, the fragments per kilobase of transcript per million mapped reads (FPKM) values, which indicate relative gene expression levels, of *DEGS1* and *DEGS2* were 186 and 32 (17% of *DEGS1*), respectively (51). On the other hand, the FPKM values of *Degs1* and *Degs2* were 95 and 0.036 (0.04% of *Degs1*) in the skin of mice (52). Although the gene responsible for the production of 6-hydroxy sphingosine-type ceramide has not yet been identified, the absence of 6-hydroxy sphingosine-type ceramide in mice suggests that the gene involved does not exist in mice or is not expressed in the skin of mice. Additionally, the FPKM value of *FA2H*, which encodes the FA 2-hydroxylase responsible for hydroxylating FAs, the substrate of nonhydroxy ceramide, to generate  $\alpha$ -hydroxy ceramide, was low in mice (0.17% of *Degs1* in mice; 4.2% of *DEGS1* in humans) (51, 52), possibly causing low levels of  $\alpha$ -hydroxy ceramides in mice. In *Fa2h* KO mice, neither the skin phenotype nor reduced AS levels in skin were observed (53). In that report, however, it is likely that BS, but not AS, was measured, because AS levels were determined by TLC or MS analysis without LC separation (53).

BS levels were increased by DKO of the  $\beta$ -hydroxy acyl-CoA dehydratase genes *HACD1* and *HACD2* in the FA elongation cycle (Fig. 6B). Because acyl-CoAs with  $\geq$ C18 chain lengths are produced in the FA elongation cycle, the high levels of BS species with  $\geq$ C18 chain lengths (Fig. 3E) may indicate that BS is synthesized in the ER by the condensation of LCB and  $\beta$ -hydroxy acyl-CoA supplied from the FA elongation cycle. However, further analyses are required, because (*R*)  $\beta$ -hydroxy acyl-CoAs are also produced as an intermediate in  $\beta$ -oxidation in peroxisomes (54) and because it is still possible that BS is generated by  $\beta$ -hydroxylation of NS by an unidentified hydroxylase. To our knowledge, no experimental evidence has been reported for the structural configuration of  $\beta$ -hydroxy acyl-CoA in FA elongation so far. In this study, we have proven, for the first time, that the  $\beta$ -hydroxy acyl-CoA produced in FA elongation has an (*R*) configuration.

Earlier studies have reported that ceramides with odd-chain FAs exist at high levels in the SC (Fig. 3F, supplemental Table S3) (7, 55). Odd-chain FAs are produced by  $\alpha$ -oxidation (cleavage of one carbon chain) of  $\alpha$ -hydroxy FAs (56). Therefore, the high C25:0 nonhydroxy and  $\alpha$ -hydroxy ceramide levels are presumed to be derived from the high levels of C26:0  $\alpha$ -hydroxy ceramide, and odd-chain FAs with chain lengths  $\geq$ C27:0 may be generated by the elongation of C25:0 acyl-CoA through the FA elongation cycle.

The amounts of EO ceramides were comparable between EOS, EOH, and EOP in the human SC (Fig. 3A), whereas those of P-O ceramides were different: P-OS was the most abundant, and P-OH and P-OP were half and 1/10 of P-OS, respectively (Fig. 4A). Because P-O ceramides are derived from EO ceramides, the difference in LCB composition between EO and P-O ceramides indicates that the conversion efficiency of EO to P-O ceramides varies depending on the LCB structure (the presence of hydroxylation), presumably due to the low activities against EOP and EOH of the enzymes involved in the production of P-O ceramides.

In this study, we revealed that the composition of ceramide classes, especially in hydroxylated ceramide classes, are different between human and mouse SC. Therefore, it is predicted that the use of mice deficient in a hydroxylase gene involved in the production of hydroxylated ceramide may not always be appropriate as a model for human skin disorders. On the other hand, the use of mice is still suitable for elucidating the importance of the common features between human and mice, including EO ceramides, P-O ceramides, and ceramides with ultra-long-chain FAs ( $\geq$ C26), in skin barrier function.

In the current study, we successfully quantified a large number of ceramide species in the SC. Although we focused on and quantified ceramide species containing LCBs with a C18 chain length, LCBs with different chain lengths (C14–C26) reportedly exist in the epidermis (57). Because it is possible to separate and quantify ceramide species having these LCBs by LC/MS/MS, more extensive SC ceramide profiles will be analyzed in future studies. By using our method to investigate and compare SC ceramide profiles from patients with skin disorders, the role of each ceramide class in skin barrier formation and the pathogenesis of skin disorders is expected to be revealed, leading to the development of therapeutic drugs. 

#### Data availability

All data are contained within the manuscript.

The authors thank Megumi Sawai for providing the *HACD1* *HACD2* DKO cells.

#### REFERENCES

1. Traupe, H., J. Fischer, and V. Oji. 2014. Nonsyndromic types of ichthyoses – an update. *J. Dtsch. Dermatol. Ges.* **12**: 109–121.
2. Borodzicz, S., L. Rudnicka, D. Mirowska-Guzel, and A. Cudnoch-Jedrzejewska. 2016. The role of epidermal sphingolipids in dermatologic diseases. *Lipids Health Dis.* **15**: 13.

3. Goleva, E., E. Berdyshev, and D. Y. Leung. 2019. Epithelial barrier repair and prevention of allergy. *J. Clin. Invest.* **129**: 1463–1474.
4. Yardley, H. J., and R. Summerly. 1981. Lipid composition and metabolism in normal and diseased epidermis. *Pharmacol. Ther.* **13**: 357–383.
5. Masukawa, Y., H. Narita, E. Shimizu, N. Kondo, Y. Sugai, T. Oba, R. Homma, J. Ishikawa, Y. Takagi, T. Kitahara, et al. 2008. Characterization of overall ceramide species in human stratum corneum. *J. Lipid Res.* **49**: 1466–1476.
6. van Smeden, J., L. Hoppel, R. van der Heijden, T. Hankemeier, R. J. Vreeken, and J. A. Bouwstra. 2011. LC/MS analysis of stratum corneum lipids: ceramide profiling and discovery. *J. Lipid Res.* **52**: 1211–1221.
7. t'Kindt, R., L. Jorge, E. Dumont, P. Couturon, P. Sandra, and K. Sandra. 2012. Profiling and characterizing skin ceramides using reversed-phase liquid chromatography-quadrupole time-of-flight mass spectrometry. *Anal. Chem.* **84**: 403–411.
8. Kihara, A. 2016. Synthesis and degradation pathways, functions, and pathology of ceramides and epidermal acylceramides. *Prog. Lipid Res.* **63**: 50–69.
9. Pruetz, S. T., A. Bushnev, K. Hagedorn, M. Adiga, C. A. Haynes, M. C. Sullards, D. C. Liotta, and A. H. Merrill, Jr. 2008. Biodiversity of sphingoid bases ("sphingosines") and related amino alcohols. *J. Lipid Res.* **49**: 1621–1639.
10. Jojima, K., M. Edagawa, M. Sawai, Y. Ohno, and A. Kihara. 2020. Biosynthesis of the anti-lipid-microdomain sphingoid base 4,14-sphingadiene by the ceramide desaturase FADS3. *FASEB J.* **34**: 3318–3335.
11. Lin, M. H., F. F. Hsu, D. Crumrine, J. Meyer, P. M. Elias, and J. H. Miner. 2019. Fatty acid transport protein 4 is required for incorporation of saturated ultralong-chain fatty acids into epidermal ceramides and monoacylglycerols. *Sci. Rep.* **9**: 13254.
12. Tsugawa, H., K. Ikeda, W. Tanaka, Y. Senoo, M. Arita, and M. Arita. 2017. Comprehensive identification of sphingolipid species by in silico retention time and tandem mass spectral library. *J. Cheminform.* **9**: 19.
13. Gray, G. M., R. J. White, and J. R. Majer. 1978. 1-(3'-O-acyl)- $\beta$ -glucosyl-N-dihydroxypentatriacontadienoylsphingosine, a major component of the glucosylceramides of pig and human epidermis. *Biochim. Biophys. Acta.* **528**: 127–137.
14. Wertz, P. W., and D. T. Downing. 1986. Linoleate content of epidermal acylglucosylceramide in newborn, growing and mature mice. *Biochim. Biophys. Acta.* **876**: 469–473.
15. Imokawa, G., A. Abe, K. Jin, Y. Higaki, M. Kawashima, and A. Hidano. 1991. Decreased level of ceramides in stratum corneum of atopic dermatitis: an etiologic factor in atopic dry skin? *J. Invest. Dermatol.* **96**: 523–526.
16. Ishikawa, J., H. Narita, N. Kondo, M. Hotta, Y. Takagi, Y. Masukawa, T. Kitahara, Y. Takema, S. Koyano, S. Yamazaki, et al. 2010. Changes in the ceramide profile of atopic dermatitis patients. *J. Invest. Dermatol.* **130**: 2511–2514.
17. Janssens, M., J. van Smeden, G. S. Gooris, W. Bras, G. Portale, P. J. Caspers, R. J. Vreeken, T. Hankemeier, S. Kezic, R. Wolterbeek, et al. 2012. Increase in short-chain ceramides correlates with an altered lipid organization and decreased barrier function in atopic eczema patients. *J. Lipid Res.* **53**: 2755–2766.
18. Bouwstra, J. A., G. S. Gooris, F. E. Dubbelaar, and M. Ponc. 2002. Phase behavior of stratum corneum lipid mixtures based on human ceramides: the role of natural and synthetic ceramide 1. *J. Invest. Dermatol.* **118**: 606–617.
19. Lundborg, M., A. Narangifard, C. L. Wennberg, E. Lindahl, B. Daneholt, and L. Norlen. 2018. Human skin barrier structure and function analyzed by cryo-EM and molecular dynamics simulation. *J. Struct. Biol.* **203**: 149–161.
20. Candi, E., R. Schmidt, and G. Melino. 2005. The cornified envelope: a model of cell death in the skin. *Nat. Rev. Mol. Cell Biol.* **6**: 328–340.
21. Elias, P. M., R. Gruber, D. Crumrine, G. Menon, M. L. Williams, J. S. Wakefield, W. M. Holleran, and Y. Uchida. 2014. Formation and functions of the corneocyte lipid envelope (CLE). *Biochim. Biophys. Acta.* **1841**: 314–318.
22. Akiyama, M. 2017. Corneocyte lipid envelope (CLE), the key structure for skin barrier function and ichthyosis pathogenesis. *J. Dermatol. Sci.* **88**: 3–9.
23. Muñoz-García, A., C. P. Thomas, D. S. Keeney, Y. Zheng, and A. R. Brash. 2014. The importance of the lipoygenase-hepoxilin pathway in the mammalian epidermal barrier. *Biochim. Biophys. Acta.* **1841**: 401–408.
24. Hirabayashi, T., T. Anjo, A. Kaneko, Y. Senoo, A. Shibata, H. Takama, K. Yokoyama, Y. Nishito, T. Ono, C. Taya, et al. 2017. PNPLA1 has a crucial role in skin barrier function by directing acylceramide biosynthesis. *Nat. Commun.* **8**: 14609.
25. Yamamoto, H., M. Hattori, W. Chamulitrat, Y. Ohno, and A. Kihara. 2020. Skin permeability barrier formation by the ichthyosis-causative gene *FATP4* through formation of the barrier lipid  $\omega$ -O-acylceramide. *Proc. Natl. Acad. Sci. USA.* **117**: 2914–2922.
26. Miyamoto, M., N. Itoh, M. Sawai, T. Sassa, and A. Kihara. 2020. Severe skin permeability barrier dysfunction in knockout mice deficient in a fatty acid  $\omega$ -hydroxylase crucial to acylceramide production. *J. Invest. Dermatol.* **140**: 319–326.e4.
27. Kihara, A. 2012. Very long-chain fatty acids: elongation, physiology and related disorders. *J. Biochem.* **152**: 387–395.
28. Edagawa, M., M. Sawai, Y. Ohno, and A. Kihara. 2018. Widespread tissue distribution and synthetic pathway of polyunsaturated C24:2 sphingolipids in mammals. *Biochim. Biophys. Acta Mol. Cell Biol. Lipids.* **1863**: 1441–1448.
29. Farwanah, H., J. Wohlrab, R. H. Neubert, and K. Raith. 2005. Profiling of human stratum corneum ceramides by means of normal phase LC/APCI-MS. *Anal. Bioanal. Chem.* **383**: 632–637.
30. Weerheim, A., and M. Ponc. 2001. Determination of stratum corneum lipid profile by tape stripping in combination with high-performance thin-layer chromatography. *Arch. Dermatol. Res.* **293**: 191–199.
31. Rabionet, M., A. Bayerle, C. Marsching, R. Jennemann, H. J. Grone, Y. Yildiz, D. Wachten, W. Shaw, J. A. Shayman, and R. Sandhoff. 2013. 1-O-acylceramides are natural components of human and mouse epidermis. *J. Lipid Res.* **54**: 3312–3321.
32. Breiden, B., and K. Sandhoff. 2014. The role of sphingolipid metabolism in cutaneous permeability barrier formation. *Biochim. Biophys. Acta.* **1841**: 441–452.
33. Nishifuji, K., and J. S. Yoon. 2013. The stratum corneum: the rampart of the mammalian body. *Vet. Dermatol.* **24**: 60–72.e15–6.
34. Sassa, T., Y. Ohno, S. Suzuki, T. Nomura, C. Nishioka, T. Kashiwagi, T. Hirayama, M. Akiyama, R. Taguchi, H. Shimizu, et al. 2013. Impaired epidermal permeability barrier in mice lacking *Elovl1*, the gene responsible for very-long-chain fatty acid production. *Mol. Cell Biol.* **33**: 2787–2796.
35. Vasireddy, V., Y. Uchida, N. Salem, Jr., S. Y. Kim, M. N. Mandal, G. B. Reddy, R. Bodepudi, N. L. Alderson, J. C. Brown, H. Hama, et al. 2007. Loss of functional *ELOVL4* depletes very long-chain fatty acids ( $\geq$ C28) and the unique  $\omega$ -O-acylceramides in skin leading to neonatal death. *Hum. Mol. Genet.* **16**: 471–482.
36. Jennemann, R., M. Rabionet, K. Gorgas, S. Epstein, A. Dalpke, U. Rothermel, A. Bayerle, F. van der Hoeven, S. Imgrund, J. Kirsch, et al. 2012. Loss of ceramide synthase 3 causes lethal skin barrier disruption. *Hum. Mol. Genet.* **21**: 586–608.
37. Aioi, A., H. Tonogaito, H. Suto, K. Hamada, C. R. Ra, H. Ogawa, H. Maibach, and H. Matsuda. 2001. Impairment of skin barrier function in NC/Nga Tnd mice as a possible model for atopic dermatitis. *Br. J. Dermatol.* **144**: 12–18.
38. Park, Y. H., W. H. Jang, J. A. Seo, M. Park, T. R. Lee, Y. H. Park, D. K. Kim, and K. M. Lim. 2012. Decrease of ceramides with very long-chain fatty acids and downregulation of elongases in a murine atopic dermatitis model. *J. Invest. Dermatol.* **132**: 476–479.
39. Ohno, Y., N. Kamiyama, S. Nakamichi, and A. Kihara. 2017. PNPLA1 is a transacylase essential for the generation of the skin barrier lipid  $\omega$ -O-acylceramide. *Nat. Commun.* **8**: 14610.
40. Carette, J. E., M. Raaben, A. C. Wong, A. S. Herbert, G. Obernosterer, N. Mulherkar, A. I. Kuehne, P. J. Kranzusch, A. M. Griffin, G. Ruthel, et al. 2011. Ebola virus entry requires the cholesterol transporter Niemann-Pick C1. *Nature.* **477**: 340–343.
41. Sawai, M., Y. Uchida, Y. Ohno, M. Miyamoto, C. Nishioka, S. Itoharu, T. Sassa, and A. Kihara. 2017. The 3-hydroxyacyl-CoA dehydratases HADC1 and HADC2 exhibit functional redundancy and are active in a wide range of fatty acid elongation pathways. *J. Biol. Chem.* **292**: 15538–15551.
42. Hsu, F. F. 2016. Complete structural characterization of ceramides as [M-H]<sup>-</sup> ions by multiple-stage linear ion trap mass spectrometry. *Biochimie.* **130**: 63–75.
43. Robson, K. J., M. E. Stewart, S. Michelsen, N. D. Lazo, and D. T. Downing. 1994. 6-Hydroxy-4-sphingenine in human epidermal ceramides. *J. Lipid Res.* **35**: 2060–2068.
44. Wertz, P. W., K. C. Madison, and D. T. Downing. 1989. Covalently bound lipids of human stratum corneum. *J. Invest. Dermatol.* **92**: 109–111.

45. Fujiwara, A., M. Morifuji, M. Kitade, K. Kawahata, T. Fukasawa, T. Yamaji, H. Itoh, and M. Kawashima. 2018. Age-related and seasonal changes in covalently bound ceramide content in forearm stratum corneum of Japanese subjects: determination of molecular species of ceramides. *Arch. Dermatol. Res.* **310**: 729–735.
46. Utsunomiya, A., T. Chino, N. Utsunomiya, V. H. Luong, A. Tokuriki, T. Naganuma, M. Arita, K. Higashi, K. Saito, N. Suzuki, et al. 2020. Homeostatic function of dermokine in the skin barrier and inflammation. *J. Invest. Dermatol.* **140**: 838–849.e9.
47. Sassa, T., and A. Kihara. 2014. Metabolism of very long-chain fatty acids: genes and pathophysiology. *Biomol. Ther. (Seoul)*. **22**: 83–92.
48. Ikeda, M., Y. Kanao, M. Yamanaka, H. Sakuraba, Y. Mizutani, Y. Igarashi, and A. Kihara. 2008. Characterization of four mammalian 3-hydroxyacyl-CoA dehydratases involved in very long-chain fatty acid synthesis. *FEBS Lett.* **582**: 2435–2440.
49. Omae, F., M. Miyazaki, A. Enomoto, M. Suzuki, Y. Suzuki, and A. Suzuki. 2004. DES2 protein is responsible for phytoceramide biosynthesis in the mouse small intestine. *Biochem. J.* **379**: 687–695.
50. Ternes, P., S. Franke, U. Zahringer, P. Sperling, and E. Heinz. 2002. Identification and characterization of a sphingolipid  $\Delta 4$ -desaturase family. *J. Biol. Chem.* **277**: 25512–25518.
51. Skaug, B., D. Khanna, W. R. Swindell, M. E. Hinchcliff, T. M. Frech, V. D. Steen, F. N. Hant, J. K. Gordon, A. A. Shah, L. Zhu, et al. 2020. Global skin gene expression analysis of early diffuse cutaneous systemic sclerosis shows a prominent innate and adaptive inflammatory profile. *Ann. Rheum. Dis.* **79**: 379–386.
52. Oberbeck, N., V. C. Pham, J. D. Webster, R. Reja, C. S. Huang, Y. Zhang, M. Roose-Girma, S. Warming, Q. Li, A. Birnberg, et al. 2019. The RIPK4–IRF6 signalling axis safeguards epidermal differentiation and barrier function. *Nature*. **574**: 249–253.
53. Maier, H., M. Meixner, D. Hartmann, R. Sandhoff, L. Wang-Eckhardt, I. Zoller, V. Gieselmann, and M. Eckhardt. 2011. Normal fur development and sebum production depends on fatty acid 2-hydroxylase expression in sebaceous glands. *J. Biol. Chem.* **286**: 25922–25934.
54. Wanders, R. J. 2004. Peroxisomes, lipid metabolism, and peroxisomal disorders. *Mol. Genet. Metab.* **83**: 16–27.
55. Masukawa, Y., H. Narita, H. Sato, A. Naoe, N. Kondo, Y. Sugai, T. Oba, R. Homma, J. Ishikawa, Y. Takagi, et al. 2009. Comprehensive quantification of ceramide species in human stratum corneum. *J. Lipid Res.* **50**: 1708–1719.
56. Kitamura, T., N. Seki, and A. Kihara. 2017. Phytosphingosine degradation pathway includes fatty acid  $\alpha$ -oxidation reactions in the endoplasmic reticulum. *Proc. Natl. Acad. Sci. USA*. **114**: E2616–E2623.
57. Pons, A., P. Timmerman, Y. Leroy, and J. P. Zanetta. 2002. Gas chromatography/mass-spectrometry analysis of human skin constituents as heptafluorobutyrate derivatives with special reference to long-chain bases. *J. Lipid Res.* **43**: 794–804.